

General and Efficient Steering of Unconditional Diffusion

Qingsong Wang Mikhail Belkin Yusu Wang

Halıcıoğlu Data Science Institute, UC San Diego

qswang92@gmail.com mbelkin@ucsd.edu yusuwang@ucsd.edu

Abstract

Guiding unconditional diffusion models typically requires either retraining with conditional inputs or per-step gradient computations (e.g., classifier-based guidance), both of which incur substantial computational overhead. We present a general recipe for efficiently steering unconditional diffusion without gradient guidance during inference, enabling fast controllable generation. Our approach is built on two observations about diffusion model structure: *Noise Alignment*: even in early, highly corrupted stages, coarse semantic steering is possible using a lightweight, offline-computed guidance signal, avoiding any per-step or per-sample gradients. *Transferable concept vectors*: a concept direction in activation space once learned transfers across both timesteps and samples; the same fixed steering vector learned near low noise level remains effective when injected at intermediate noise levels for every generation trajectory, providing refined conditional control with efficiency. Such concept directions can be efficiently and reliably identified via Recursive Feature Machine (RFM), a light-weight backpropagation-free feature learning method. Experiments on CIFAR-10, ImageNet, and CelebA demonstrate improved accuracy/quality over gradient-based guidance, while achieving significant inference speedups.

1 Introduction

Diffusion models [Ho et al., 2020, Song et al., 2021b] have become the dominant methodology for high-quality image synthesis. While unconditional models can generate diverse samples, many applications require controllable generation toward specific attributes or concepts. Classifier-free guidance [Ho and Salimans, 2022] is a popular and effective approach that enables high-quality conditional generation by incorporating the conditioning information during training. However, a key challenge arises when controlling generation at inference time for attributes beyond those seen during training diffusion models, without expensive retraining.

Popular approaches for steering unconditional models use gradients from classifiers to guide generation toward desired concepts. This includes both training-time approaches that train *noise-conditioned classifiers* [Dhariwal and Nichol, 2021, Song et al., 2021b] trained to predict labels from noisy images at different timesteps, and *training-free methods* that use pre-existing off-the-shelf classifiers [He et al., 2024, Song et al., 2023, Chung et al., 2023, Bansal et al., 2023, Yu et al., 2023, Ye et al., 2024]. Both noise-conditioned classifier and training free guidance require per-step gradient computation and for many variants need to backpropagate through the diffusion model during inference.

In this paper we develop a general framework to efficiently steer unconditional diffusion models without gradient information at inference time. Our approach is built on the following key empirical findings:

1. class information emerges early in the diffusion model inference process and can be recovered even from the pure noise stage.

2. strong class discriminative directions in activation space of the model can be transferred across a range of timesteps.
3. these discriminative directions can be used to steer models effectively.

Our work leverages these observations to amplify the discriminative signals to steer diffusion models toward target concepts efficiently. Specifically, we use two complementary steering mechanisms in image generation:

- **Early Stage (high noise).** Noise alignment via data covariance, which provides coarse semantic steering effective at early timesteps, efficiently anchoring generation toward target concepts;
- **Later Stage (low noise).** We identify steering direction by using Recursive Feature Machines (RFMs) [Radhakrishnan et al., 2024] at a certain low noise time step and apply them across all later stage time steps.

Both mechanisms **do not require classifier gradients at inference** – the directions (steering vectors) are pre-computed offline, and steering requires only vector operations at each timestep, yielding substantial speedup over training-free gradient-based methods. Furthermore, we observed significantly and consistently higher accuracy for image generations. In contrast, while noise-conditioned classifiers are almost as efficient to run, they require multiple rounds of training to classify noisy images, which makes them computationally costly to construct. For example, in Table 2, on CIFAR-10, our method achieves 96.6% guidance accuracy compared to 77.1% for SoTA Training Free Guidance (TFG) [Ye et al., 2024], and even outperforms noise-conditioned classifier guidance (86.0% accuracy), while also delivering better image quality (per-class FID 41.4 vs 73.9 vs 47.0) and 16.4 \times inference speedup over TFG. Such performance and fidelity gains over the SoTA training-free guidance also extends to ImageNet 256 \times 256, multi-attribute CelebA guidance, and generalizes to out-of-distribution fine-grained concepts; see Section 4. The efficiency gains come from eliminating per-step gradient computation—our method uses only forward passes with pre-computed directions, while gradient methods require backpropagation through both the diffusion model and classifier at every step. The fidelity gains stem from our method’s principled approach to identifying the key concept direction that steers the object while making minimal changes to the output.

In summary, we propose an efficient and effective gradient-free framework to steer unconditional diffusion models at inference time. It combines high-noise noise alignment with later stage RFM-learned concept steering, enabling fast sampling with strong control accuracy and image quality. Extensive experiments show that our approaches are not only more accurate but also more efficient than prior methods for steering unconditional diffusion models.

2 Background and Related Work

2.1 Diffusion Models

Diffusion models [Ho et al., 2020, Song et al., 2021b] are trained by learning to denoise noisy inputs at various timesteps; generation then samples through the learned denoising process. The **forward (noising) process** linearly mixes clean data \mathbf{x}_0 with Gaussian noise over timesteps $t = 0, \dots, T$ [Karras et al., 2022]:

$$\mathbf{x}_t = \alpha_t \mathbf{x}_0 + \beta_t \boldsymbol{\epsilon}, \quad \boldsymbol{\epsilon} \sim \mathcal{N}(\mathbf{0}, \mathbf{I}), \quad (1)$$

where $\alpha_t = \sqrt{\bar{\alpha}_t}$ and $\beta_t = \sqrt{1 - \bar{\alpha}_t}$ define a noise schedule with $\alpha_0 = 1$, $\beta_0 = 0$ (clean data) and $\alpha_T \approx 0$, $\beta_T \approx 1$ (pure noise). During training, the denoiser $\epsilon_\theta(\mathbf{x}_t, t)$ is optimized to predict the

injected noise ϵ at each timestep. The **reverse process** learns to iteratively denoise, enabling generation by transforming random noise back into data. During training, a neural network $\epsilon_\theta(\mathbf{x}_t, t)$ is optimized to predict the noise component ϵ added during the forward process. At sampling time, we start from pure noise $\mathbf{x}_T \sim \mathcal{N}(\mathbf{0}, \mathbf{I})$ and apply a deterministic DDIM update (Eq. 3).

A key quantity for guidance methods is the **denoised estimate** at timestep t :

$$\hat{\mathbf{x}}_0^{(t)} = \frac{\mathbf{x}_t - \beta_t \epsilon_\theta(\mathbf{x}_t, t)}{\alpha_t}, \quad (2)$$

which represents the model’s best prediction of the clean image \mathbf{x}_0 given the current noisy state \mathbf{x}_t . This quantity provides a direct estimate of the final output at any intermediate timestep, making it central to many guidance mechanisms. The reverse process can be sampled using DDIM [Song et al., 2021a]. The DDIM update with noise level η is:

$$\mathbf{x}_{t-1} = \alpha_{t-1} \hat{\mathbf{x}}_0^{(t)} + \sqrt{\beta_{t-1}^2 - \sigma_t^2} \epsilon_\theta(\mathbf{x}_t, t) + \sigma_t \mathbf{z}, \quad (3)$$

where $\sigma_t = \eta \cdot \frac{\beta_{t-1}}{\beta_t} \sqrt{1 - \frac{\alpha_t^2}{\alpha_{t-1}^2}}$, and $\mathbf{z} \sim \mathcal{N}(\mathbf{0}, \mathbf{I})$. Setting $\eta = 0$ recovers the deterministic ODE sampler.

Remark. For a fixed noise schedule, predicting noise ϵ , the denoised data \mathbf{x}_0 , the velocity v , or the score $\nabla_{\mathbf{x}_t} \log p_t(\mathbf{x}_t)$ are equivalent parameterizations related by simple linear transforms, so guidance can be expressed in any of these forms. The same discussion applies to flow-matching/ODE formulations [Song et al., 2021b, Lipman et al., 2024].

Classifier Guidance [Dhariwal and Nichol, 2021] steers generation by modifying the noise prediction using gradients from a noise-conditioned classifier $p_\phi(y|\mathbf{x}_t)$ trained on noisy images at all timesteps:

$$\tilde{\epsilon}_\theta(\mathbf{x}_t, t, y) = \epsilon_\theta(\mathbf{x}_t, t) - \sqrt{1 - \bar{\alpha}_t} \cdot w \nabla_{\mathbf{x}_t} \log p_\phi(y|\mathbf{x}_t). \quad (4)$$

The gradient $\nabla_{\mathbf{x}_t} \log p_\phi(y|\mathbf{x}_t)$ gives a direction in pixel space that increases the probability of class y , applied to the noise prediction before computing \mathbf{x}_{t-1} . This approach requires: (1) training noise-conditioned classifiers for each timestep which requires multiple training epochs and high computational cost, and (2) backpropagating through the classifier at *every* denoising step during inference.

Classifier-Free Guidance (CFG) [Ho and Salimans, 2022] eliminates the need for an auxiliary classifier by training a single conditional model $\epsilon_\theta(\mathbf{x}_t, t, c)$ with random condition dropout (denoted by \emptyset). At inference, guidance is achieved by modifying the noise prediction through interpolation:

$$\tilde{\epsilon}_\theta = \epsilon_\theta(\mathbf{x}_t, t, \emptyset) + w \cdot (\epsilon_\theta(\mathbf{x}_t, t, c) - \epsilon_\theta(\mathbf{x}_t, t, \emptyset)). \quad (5)$$

While elegant and widely used, this requires conditioning at training time, providing limited post-hoc controllability for attributes not seen during training.

Training-Free Gradient-based Guidance. To enable post-hoc control without retraining, several methods use off-the-shelf classifiers trained on clean images and backpropagate guidance from either \mathbf{x}_t or the denoised estimate $\hat{\mathbf{x}}_0^{(t)}$ at each step [Bansal et al., 2023, Yu et al., 2023, Ye et al., 2024]. Representative lines include inverse-problem solvers such as DPS,LGD [Chung et al., 2023, Song et al., 2023], iterative refinement strategies like FreeDoM, and variants that guide through $\hat{\mathbf{x}}_0^{(t)}$ or add backward optimization (e.g., MPGD, UGD) [Yu et al., 2023, He et al., 2024, Bansal et al., 2023, Ye et al., 2024]. Despite their differences, these methods share two limitations: clean-trained classifiers provide weak or misaligned gradients at high noise (often addressed with

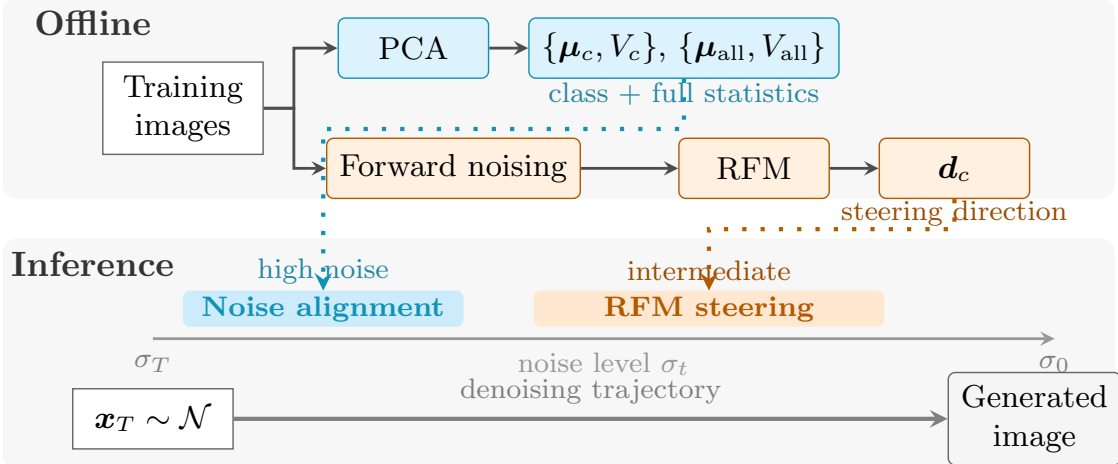


Figure 1: **Overview of Noise-Aligned RFM Steering.** *Offline:* We compute class-conditional PCA statistics (cyan) and extract RFM steering directions from forward-process activations (orange). *Inference:* During sampling, we apply noise alignment at high noise levels to establish coarse class structure, then RFM steering at intermediate noise for fine-grained discriminative control. The two mechanisms require no classifier gradients at inference time.

extra refinement steps), and per-step backpropagation makes sampling substantially slower than unconditional generation.

Activation Steering. In diffusion models, the U-Net bottleneck features (“h-space”) have been shown to act as a semantic latent space and support linear, interpretable edits [Kwon et al., 2023]. Follow-up work uses h-space feature manipulation for training-free content injection and editing [Jeong et al., 2024]. These approaches highlight that internal activations can remain semantically meaningful even when pixel-level patterns are corrupted by noise. In our experiments, however, the encoder block immediately before the bottleneck yields stronger steerability than the bottleneck itself. Comparing with our approach, these activation steering methods in diffusion models often focus on single-image editing rather than class-level guidance, and typically require DDIM inversion which we do not use.

3 Method: Noise-Aligned RFM Steering

Recursive Feature Machines (RFMs) have shown great success in concept steering in Large Language Models [Beaglehole et al., 2025] and autoregressive models [Zhao et al., 2025], where they identify discriminative directions in the activation space that enable precise control over generated content **without** per-token gradient computation. Diffusion models similarly possess rich internal activation semantics, e.g, the bottleneck features in the activation space of U-Net [Kwon et al., 2023]. This motivates us to adapt RFM-based activation steering to diffusion models for class-conditional generation, providing a gradient-free alternative to pixel-space guidance methods. However, as we will see below, we will not use RFM-based steering across entire inference trajectories, and instead, develop an efficient 2-stage steering mechanism. In what follows, we first provides some empirical findings that motivates our approach (Section 3.1), and then describe details in Sections 3.2 to 3.4.

3.1 Method overview and motivating findings

Method overview. We separate one-time offline computation from lightweight inference-time guidance. **Offline step:** we (i) compute class-conditional PCA statistics for noise alignment and (ii) collect forward-process activations at clean timesteps to train RFMs and extract per-class steering directions. **At inference**, we deploy a simple two-stage steering mechanism: we sample normally but apply *noise alignment* at high noise and *RFM steering* at intermediate/late timesteps. Both steering strategies are light-weight and do not require any inference-time gradient computation (only simple vector operations). We will see that noise-alignment steering is done in the pixel space for fast coarse adjustment, while RFM-steering happens in the activation space of denoisers network instead of pixel space, as a discriminative linearized guide signal is more likely to be found in the semantic-rich activation space. An overview of the method is shown in Figure 1. Details are given in Section 3.2 and Section 3.3, and the full inference procedure is summarized in Algorithm 1 (see also Section 3.4).

Motivation. Diffusion models denoise over many timesteps, and the amount of class information in activations varies with the noise level. This raises two practical design questions: **when** along the trajectory is activation steering effective, and **how** can we discover class directions efficiently? We answer these by probing class information across timesteps and neural network layers in the diffusion model architecture to capture the concept subspace in the **activation space**.

When there are many classes (e.g., ImageNet-1K) or rare concepts, collecting activations along full reverse sampling trajectories can be prohibitive—generating enough samples to observe a target class requires running many costly denoising steps. In contrast, labeled data is often abundant, and the forward process can directly target specific noise levels to obtain the corresponding activations, without needing to go through intermediate levels like in the reverse process. This motivates a careful choice of *where* to collect activations and whether the much cheaper forward-process noising can substitute for the much more expensive reverse sampling without sacrificing discriminability.

Probing experiments. To map where class information exists, we train linear classifiers on U-Net activations from 10,000 samples across timesteps and neural network blocks (we focus on the 4×4 and 8×8 decoder blocks, which are deeper and show the strongest class signal; results are consistent across blocks). The forward process collects activations from noisy images generated by adding noise to real images, while the reverse process collects activations along DDIM sampling trajectories starting from pure noise.

Figure 2 reveals complementary patterns across the two processes. Reverse (sampling) activations encode meaningful class information even at the earliest steps ($\sim 35\%$ accuracy), while forward (noising) activations are highly discriminative at late/clean timesteps ($\sim 80\%+$) but drop to random performance at early timesteps ($\sim 10\%$). These findings motivate our hybrid approach: utilizing noise alignment in the early stages where structural information is coarse, and RFM steering in later stages where fine-grained semantic directions are available.

We note that the above asymmetry stems from the deterministic reverse ODE (e.g., DDIM): each noise sample maps uniquely to a specific image, so the trajectory inherently encodes the target class. Even at high noise levels, the model’s activations reflect where the sampling trajectory will end up. In contrast, forward noising adds i.i.d. Gaussian noise, so at high noise $\mathbf{x}_t \approx \epsilon$ and class structure is largely destroyed.

Design choice 1: Learn directions from clean forward activations. Collecting activations from reverse sampling trajectories is expensive—for 1,000 samples with 100 DDIM steps this means 100,000 U-Net evaluations, most of which are redundant if we only need directions at a few timesteps. Forward-process collection requires only one forward pass per image. Since forward activations at clean timesteps are highly discriminative, we perform our RFM-based feature direction discovery

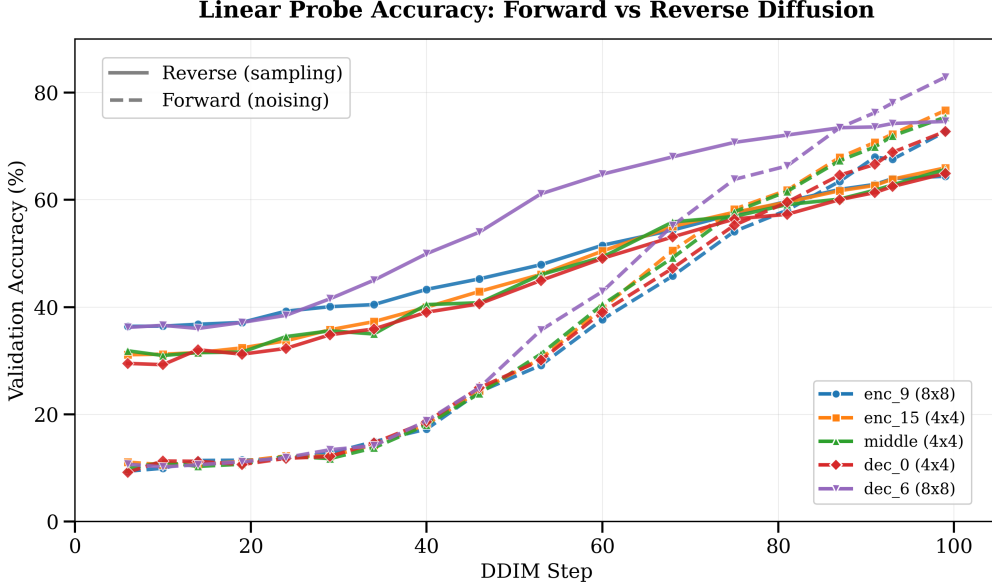


Figure 2: **Linear probe accuracy on forward vs reverse diffusion activations.** We probe U-Net activations by training linear classifiers on features collected during reverse (sampling, solid lines) and forward (noising, dashed lines) processes across 5 representative blocks within U-Net architecture.

(Section 3.3) there. Our experiments in Section 4 validate the effectiveness of this choice. Crucially, consistent with Figure 2, forward activations are most informative at low noise levels (late timesteps), so we extract directions from this regime.

Design choice 2: Reuse / transfer clean-time directions across intermediate timesteps. We measure cosine similarity between RFM directions learned at different timesteps. Figure 3 shows that directions from late/clean timesteps (e.g., noise level ≈ 0.21 for CIFAR-10) align well with intermediate timesteps during sampling, especially in encoder blocks as indicated by the large red-colored submatrix in the heatmap. This temporal transfer lets us apply a **single** clean-time direction across the guidance window, avoiding per-step RFM computation without hurting performance (and occasionally improving it in ablations).

Note that Figure 3 also shows that the earliest timesteps deviate substantially from clean-time directions. Recall that Figure 2 shows that forward activations at high noise are near-random. Together, this means clean-time RFM directions do not provide reliable steering in the initial stage, motivating a separate early-stage (high noise) mechanism.

In what follows, we describe our guidance strategy for the early stage (high noise) and late stage (low noise).

3.2 Guidance for early stage: Noise alignment.

At high noise, prior work finds diffusion scores are well-approximated by Gaussian/linear structure, so fine-grained patterns are lost but coarse class statistics remain. [Wang and Vastola, 2024]. We leverage this by computing the optimal linear denoiser for a Gaussian distribution (PCA shrinkage) in PCA space: [Li et al., 2024, 2025]

$$D_c(\mathbf{x}_t; \sigma_t) = \boldsymbol{\mu}_c + V_c \text{diag} \left(\frac{\lambda_j}{\lambda_j + \sigma_t^2} \right) V_c^\top (\mathbf{x}_t - \boldsymbol{\mu}_c), \quad (6)$$

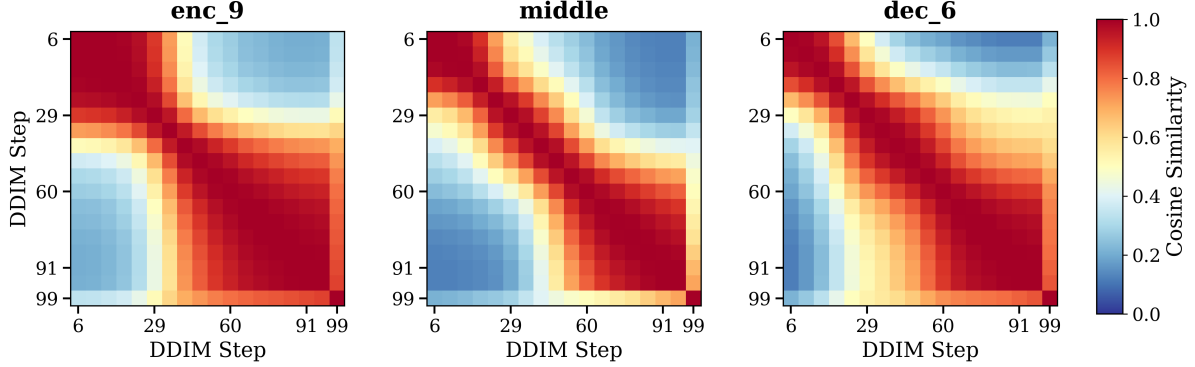


Figure 3: **Temporal transfer of RFM directions.** Cosine similarity heatmaps across three representative blocks show that directions exhibits temporal similarity for later stage blocks. x - and y -axis are diffusion timesteps, increasing top-down and left-right. The encoder block (left) exhibit the highest temporal stability with highest corss-time step cosine similarity, followed by decoder blocks (right) and middle blocks (middle).

where $\{\boldsymbol{\mu}_c, V_c, \Lambda_c\}$ are the PCA components of class c training data, and σ_t is the noise level. Similarly, we compute an unconditional denoiser $D_{\text{all}}(\mathbf{x}_t; \sigma_t)$ using full dataset statistics $\{\boldsymbol{\mu}_{\text{all}}, V_{\text{all}}, \Lambda_{\text{all}}\}$.

The guidance signal is the difference between conditional and unconditional denoisers:

$$\mathbf{g}_t^{\text{Gauss}} = D_c(\mathbf{x}_t; \sigma_t) - D_{\text{all}}(\mathbf{x}_t; \sigma_t). \quad (7)$$

It turns out that the difference of Gaussian alone can already effectively steer the diffusion model, as shown in Figure 8.

This requires no training – just precomputed class statistics – and works precisely where activation steering fails due to the lack of fine-grained semantic signal in high-noise activations (Figure 2, top-left). Note that these statistics are computed only once per class.

3.3 Guidance in late stage: RFM-Based direction discovery and transfer

Guided by the probing results, we discover semantic directions using *forward-process* activations at clean timesteps using Recursive Feature Machines (RFMs) [Radhakrishnan et al., 2024]. Given a dataset of images $\{(\mathbf{x}_i, y_i)\}$, we collect U-Net activations during one-step forward noising:

$$\mathbf{h}_i = \phi(\mathbf{x}_t^{(i)}, t), \quad \mathbf{x}_t^{(i)} = \sqrt{\bar{\alpha}_t} \mathbf{x}_i + \sqrt{1 - \bar{\alpha}_t} \boldsymbol{\epsilon}, \quad (8)$$

where $\phi(\cdot, t)$ extracts intermediate activations at block ℓ (omitted for brevity) and timestep t . We use the last encoder block before the bottleneck in U-Net, which appears most effective because modifications propagate to decoder blocks via skip connections.

RFM Training. Given activations $\{\mathbf{h}_i\}$ from a chosen U-Net block and binary labels indicating the target class, RFM *iteratively* learns a discriminative direction: **(1) Kernel construction.** We build a Laplacian kernel $K_{ij} = \exp(-\gamma d_M(\mathbf{h}_i, \mathbf{h}_j))$ where the Mahalanobis distance d_M is parameterized by matrix M , and γ is the bandwidth of the kernel. Initially $M = I$ (Euclidean distance). **(2) AGOP update.**

After solving kernel ridge regression with predictor f , we compute function gradients $\mathbf{g}_i = \nabla_{\mathbf{h}} f(\mathbf{h}_i)$. The AGOP matrix $M^{\text{AGOP}} = \frac{1}{N} \sum_i \mathbf{g}_i \mathbf{g}_i^\top$ captures which directions most influence the classifier. This becomes the new M for the next iteration. **(3) Iterative**

refinement. Steps (1)–(2) repeat for T iterations. Each iteration refines M : the kernel adapts to emphasize discriminative features, which produces better gradients, which further improves M . This bootstrapping enables feature learning within the kernel framework without backpropagation.

(4) RFM Steering direction. After convergence, the top eigenvector of the final AGOP gives the *steering direction* \mathbf{v}_c —the single direction in activation space that most discriminates class c from others. We use weighted average of top- k eigenvectors by eigenvalues with k often equals 1, 3 or 5. Once the direction is computed, we use it to steer the generation process.

Steering Application. During inference, we steer the model’s activations \mathbf{h} by

$$\mathbf{h}_{\text{steered}}^{(\ell)} = \mathbf{h}^{(\ell)} + w_{\text{RFM}} \|\mathbf{h}^{(\ell)}\| \mathbf{v}_c \quad (9)$$

where w_{RFM} is the steering strength. Note we use the norm of the activations to scale the steering direction to have comparable magnitudes with activations.

CFG-Style Boosting. After steering activations via Equation (9), we obtain a steered noise prediction ϵ_{rfm} and corresponding denoised estimate $\hat{\mathbf{x}}_0^{\text{rfm}}$. To amplify the steering effect, we apply a classifier-free guidance (CFG) style update:

$$\hat{\mathbf{x}}_0 \leftarrow \hat{\mathbf{x}}_0 + s \cdot (\hat{\mathbf{x}}_0^{\text{rfm}} - \hat{\mathbf{x}}_0) \quad (10)$$

where s is the CFG scale. This strengthens the guidance signal.

3.4 Inference

At inference time, we steer generation with stage-dependent guidance: noise alignment at high noise for coarse semantic structure, then RFM steering at intermediate/late timesteps where discriminative structure is strongest. Both mechanisms use pre-computed vectors (PCA components or RFM directions), requiring only simple vector arithmetic at each step. This avoids the expensive backpropagation required by gradient-based methods. A complete sampling procedure is detailed in Algorithm 1

Computational Complexity. Offline preparation has three stages: (1) activation collection—a single forward pass per training image at the target noise level, shared across all classes (~ 1500 images/minute on one A100); (2) PCA to obtain principal components (~ 6 s for 30k samples, ~ 18 s for 150k, using GPU-accelerated randomized SVD); and (3) per-class RFM training with 5 iterations on ~ 16 k samples (~ 1 minute each). For high-dimensional activations (e.g., $D=65536$ for 256-channel 16×16 feature maps), we exploit the dual formulation: since the number of data samples $N \approx 16$ k $\ll D$, we compute the $N \times N$ Gram matrix of gradients and recover eigenvectors via the kernel trick, avoiding the more expensive $D \times D$ AGOP matrix. At inference time, our method adds only negligible overhead (two matrix-vector products for PCA, one vector addition for RFM) per guided step. Complexity is $O(1)$ forward passes per step, identical to standard CFG but without backpropagation. In contrast, gradient-based guidance requires backpropagating through the U-Net ($O(\text{depth})$ operations) at every step.

In our ImageNet experiments (4 classes), offline preparation totals ~ 15 GPU-minutes. Notably, our one-time activation collection (15k forward passes) is amortized across all classes and samples; in contrast, the SOTA method TFG-4 with best performance configurations [Ye et al., 2024] requires ~ 800 forward passes *per generated sample*, so generating just 35 samples already exceeds our offline activation collection cost. At inference (batch size 4), our method generates a batch in ~ 31.6 s compared to ~ 318.8 s for TFG-4 (4 recurrences for best performance), yielding $10\times$ speedup.

Algorithm 1 Guided Sampling with Gaussian Denoiser + RFM Steering

Require: PCA denoisers D_c, D_{all} ; RFM direction \mathbf{v}_c for block ℓ
Require: Noise alignment strength λ ; Noise alignment window end σ_{end}
Require: RFM strength w_{RFM} ; RFM window $[\sigma_{\text{R}}^{\text{lo}}, \sigma_{\text{R}}^{\text{hi}}]$; CFG scale s

- 1: $\mathbf{x}_T \sim \mathcal{N}(0, \mathbf{I})$
- 2: **for** $t = T, \dots, 1$ **do**
- 3: $\bar{\alpha}_t \leftarrow$ cumulative noise schedule;
 $\sigma_t \leftarrow \sqrt{(1 - \bar{\alpha}_t) / \bar{\alpha}_t}$
- 4: $\epsilon \leftarrow \epsilon_{\theta}(\mathbf{x}_t, t)$ {forward pass without hook}
- 5: $\hat{\mathbf{x}}_0 \leftarrow (\mathbf{x}_t - \sqrt{1 - \bar{\alpha}_t} \epsilon) / \sqrt{\bar{\alpha}_t}$
- 6: ▷ RFM steering with CFG
- 7: **if** $\sigma_t \in [\sigma_{\text{R}}^{\text{lo}}, \sigma_{\text{R}}^{\text{hi}}]$ **then**
- 8: RFM steering of activations: $\mathbf{h}^{(\ell)} \leftarrow \mathbf{h}^{(\ell)} + w_{\text{RFM}} \|\mathbf{h}^{(\ell)}\| \mathbf{v}_c$
- 9: $\epsilon_{\text{rfm}} \leftarrow \epsilon_{\theta}(\mathbf{x}_t, t)$ {forward pass with steered activations}
- 10: $\hat{\mathbf{x}}_0^{\text{rfm}} \leftarrow (\mathbf{x}_t - \sqrt{1 - \bar{\alpha}_t} \epsilon_{\text{rfm}}) / \sqrt{\bar{\alpha}_t}$
- 11: $\hat{\mathbf{x}}_0 \leftarrow \hat{\mathbf{x}}_0 + s \cdot (\hat{\mathbf{x}}_0^{\text{rfm}} - \hat{\mathbf{x}}_0)$
- 12: **end if**
- 13: ▷ Noise Alignment
- 14: **if** $\sigma_t \geq \sigma_{\text{end}}$ **then**
- 15: $\hat{\mathbf{x}}_0 \leftarrow \hat{\mathbf{x}}_0 + \lambda \cdot (D_c(\mathbf{x}_t, \sigma_t) - D_{\text{all}}(\mathbf{x}_t, \sigma_t))$
- 16: **end if**
- 17: $\epsilon \leftarrow (\mathbf{x}_t - \sqrt{\bar{\alpha}_t} \hat{\mathbf{x}}_0) / \sqrt{1 - \bar{\alpha}_t}$
- 18: $\mathbf{x}_{t-1} \leftarrow \sqrt{\bar{\alpha}_{t-1}} \hat{\mathbf{x}}_0 + \sqrt{1 - \bar{\alpha}_{t-1}} \epsilon$ {DDIM, $\eta=0$ }
- 19: **end for**
- 20: **return** \mathbf{x}_0

4 Experiments

Table 1 summarizes our main results across all benchmarks. NA-RFM consistently outperforms all training-free baselines, including TFG-4: **+23%** relative improvement on CIFAR-10 (96.6% vs 77.1%), **+27%** on ImageNet (75.8% vs 59.8%), and **+541%** on fine-grained guidance (14.1% vs 2.2%). Crucially, NA-RFM requires **zero** classifier evaluations at inference, compared to ~ 800 evaluations for TFG with recurrence, enabling 10 \times faster generation (Section A).

We evaluate NA-RFM (**Noise-Aligned RFM Steering**) across four settings introduced in TFG [Ye et al., 2024]: (1) CIFAR-10 [Krizhevsky et al., 2009] label guidance as a controlled benchmark, (2) ImageNet 256 \times 256 [Russakovsky et al., 2015] to demonstrate scaling, (3) CelebA [Karras et al., 2017] multi-attribute guidance for correlated concepts, and (4) fine-grained bird species guidance for out-of-distribution generalization. Our primary baseline is Training-Free Guidance (TFG) [Ye et al., 2024], a recent state-of-the-art gradient-based guidance method.

Datasets. We evaluate on four benchmark datasets: (1) **CIFAR-10** [Krizhevsky et al., 2009]: 32 \times 32 images across 10 classes. (2) **ImageNet** [Russakovsky et al., 2015]: 256 \times 256 images; following Ye et al. [2024], we evaluate on classes 111, 222, 333, and 444. (3) **CelebA-HQ** [Karras et al., 2017]: 256 \times 256 facial images for multi-attribute guidance (gender, age, hair color). (4) **Birds-525**: fine-grained species for out-of-distribution guidance using *ImageNet diffusion model*.

Diffusion Models. For CIFAR-10, we use the improved DDPM U-Net [Nichol and Dhariwal, 2021]. For ImageNet, we use the unconditional ADM model [Dhariwal and Nichol, 2021]. For CelebA-HQ, we use a DDPM trained on CelebA-HQ. All our methods use DDIM [Song et al., 2021a] sampling

Table 1: **Overall comparison with training-free guidance methods.** Each cell shows *accuracy* (%) / *quality metric* (FID \downarrow or KID \downarrow). Noise-Aligned RFM Steering achieves substantially higher accuracy on all tasks while requiring **zero** classifier evaluations at inference. TFG results from Ye et al. [2024]. Best in **bold**, second best accuracies underlined.

Task	DPS	LGD	FreeDoM	MPGD	UGD	TFG-1	TFG-4	NA-RFM
CIFAR-10	50.1 / 172	32.2 / 102	34.8 / 135	38.0 / 88	45.9 / 94	52.0 / 92	<u>77.1</u> / 74	96.6 / 41
ImageNet	38.8 / 193	11.5 / 210	19.7 / 200	6.8 / 239	25.5 / 205	40.9 / 176	<u>59.8</u> / 165	75.8 / 98
Gender+Age	71.6 / -4.3	52.0 / -5.1	68.7 / -3.9	68.6 / -4.8	75.1 / -4.4	<u>75.2</u> / -3.9	—	96.0 / -2.0
Gender+Hair	73.0 / -3.9	55.0 / -5.0	67.1 / -3.5	63.9 / -4.3	71.3 / -4.1	<u>76.0</u> / -3.6	—	83.3 / -2.4
Fine-grained	0.0 / 348	0.5 / 246	0.6 / 258	0.6 / 249	1.1 / 255	1.3 / 256	<u>2.2</u> / 259	14.1 / 72

Table 2: **CIFAR-10 label guidance comparison.** Noise-Aligned RFM Steering achieves the highest accuracy and lowest FID. Timing measured on A100 GPU for 16 samples with 100 DDIM steps.

Method	Acc. \uparrow	FID \downarrow	Time
TFG-4	77.1%	73.9	101.7s
Classifier-Guidance	86.0%	47.0	6.9s
Noise align. only ($\lambda=3$)	62%	99	5.8s
Noise align. only ($\lambda=8$)	80%	120	5.8s
RFM only	94.8%	40.3	6.8s
NA-RFM	96.6%	41.4	6.2s

with $T = 100$ steps and $\eta = 0$ (deterministic). Model checkpoints are listed in Section E.

Guidance and Evaluation Classifiers. In most cases the data we use is already labeled, the only exception is CelebA-HQ where we use the classifier used for guidance in the baseline TFG [Ye et al., 2024] to label the data and we use their provided eval classifier for evaluating the generated images. In all cases, we use the evaluation classifiers provided by the authors of the baseline methods. This separation prevents inflated results. Full classifier details in Section E.

Direction Discovery. We collect U-Net activations at the last block of the encoder before the bottleneck at low noise levels (DDIM step 93 out of 100 DDIM steps for CIFAR-10; $\sigma \approx 1.0$ for ImageNet/CelebA). We train binary RFM classifiers using the ℓ_2 kernel (bandwidth 100–200, regularization 10^{-3} – 10^{-4} , 5 iterations), extracting top AGOP eigenvectors as RFM directions. See Section E for per-dataset details.

Baselines. Our primary baseline is **TFG** [Ye et al., 2024], a state-of-the-art training-free guidance method. We compare against TFG with their hyperparameter $N_{\text{recur}} = 1$ (TFG-1) and $N_{\text{recur}} = 4$ (TFG-4). TFG-4 is four times more expensive than TFG-1 and often achieves better performance.

Evaluation Metrics. We use the following metrics: **Accuracy**: fraction of generated images classified as target class by an independent evaluation classifier. **FID** [Heusel et al., 2017]: Fréchet Inception Distance (smaller is better). **KID** [Bińkowski et al., 2018]: Kernel Inception Distance (log scale for CelebA) (smaller is better).

4.1 CIFAR-10: Controlled Benchmark

Table 2 presents CIFAR-10 results with 2048 samples per class. NA-RFM achieves **96.6%** guidance accuracy, substantially outperforming TFG-4 (77.1%) and Classifier-Guidance [Nichol and Dhariwal, 2021] (86.0%). NA-RFM also achieves strong image quality with FID of 41.4, compared to 47.0

Table 3: **CelebA Multi-Attribute Guidance: Gender + Hair.** Comparison with reported score from TFG [Ye et al., 2024] on gender and hair color combinations (256 samples). Our method outperforms TFG on 3 out of 4 combinations, with the largest improvement of +21.7% on the rare Male+Blond combination.

Attributes	TFG-4	Ours
Female + Non-Blond	92.2%	86.4%
Female + Blond	72.7%	80.1%
Male + Non-Blond	89.8%	98.4%
Male + Blond	46.7%	68.4%
Average	75.4%	83.3%

for Classifier-Guidance and 73.9 for TFG, while being **16× faster** than TFG. We include in Appendix Section D.3 per-class accuracy and FID breakdowns.

4.2 ImageNet: Scaling to Higher Resolution

To test scalability, we apply NA-RFM to ImageNet 256×256 using the unconditional ADM model [Dhariwal and Nichol, 2021], evaluating on 256 samples per class. As shown in Table 1, our method achieves **75.8%** average accuracy compared to TFG-4’s reported 59.8%.

Per-Class Analysis. On *nematode* (111), we achieve **83.2%** accuracy, demonstrating effective guidance on this challenging class. For the fine-grained *kuvasz* dog breed (222), we achieve 30.5% top-1 accuracy with 74.2% top-5. The top 4 predicted classes (71.1% of samples) are all large, light-colored, fluffy dogs—*kuvasz*, *malamute*, *Great Pyrenees*, and *Eskimo dog*—demonstrating successful semantic steering with confusion only among highly similar breeds. *Hamster* (333) reaches **91.8%** accuracy, and *tandem bicycle* (444) achieves **97.7%** accuracy, demonstrating near-perfect guidance on structured object classes.

4.3 CelebA: Multi-Attribute Guidance

Multi-attribute guidance is challenging because attributes are correlated in training data. For example, 97% of blonde samples are female, so the “blonde” direction implicitly encodes “female”.

Combining two directions. For each attribute (e.g., male, blond), we extract a guidance direction via linear probing on diffusion activations as a weighted combination of the top-5 eigenvectors. We then add the directions with independent strengths, e.g., male and blond:

$$\text{activation} \leftarrow \text{activation} + \alpha_{\text{male}} \cdot \mathbf{v}_{\text{male}} + \alpha_{\text{blond}} \cdot \mathbf{v}_{\text{blond}} \quad (11)$$

where $\alpha_{\text{male}}, \alpha_{\text{blond}}$ are per-attribute guidance strengths. Training two attributes doubles direction training cost but adds negligible inference compute; we similarly combine Gaussian guidance.

Tables 3 and 4 present our multi-attribute guidance results. Our method achieves superior performance on **7 out of 8** attribute combinations, with an average improvement of **+10.8 percentage points** (89.7% vs 78.8%). Notable achievements include two tasks reaching **perfect 100% accuracy** (Young+Female, Old+Male) and the largest improvement of **+30.9%** on the challenging Old+Male combination. We note the only task where TFG outperforms our method is in Female + Non-Blond.

Rare Combinations. The Male+Blond combination represents only 1% of the CelebA training data, yet our method achieves 68.4% accuracy (+21.7% over TFG). This demonstrates effective

Table 4: **CelebA Multi-Attribute Guidance: Gender + Age.** Comparison with TFG on gender and age combinations (256 samples). Our method achieves superior performance on all 4 combinations, including two perfect 100% accuracy cases.

Attributes	TFG	Ours
Young + Female	92.9%	100.0%
Old + Female	73.6%	85.2%
Young + Male	93.6%	98.8%
Old + Male	69.1%	100.0%
Average	82.3%	96.0%

Table 5: **Fine-grained bird species guidance (OOD).** Our NA-RFM achieves strong target accuracy for species not in ImageNet using deterministic DDIM sampling ($\eta=0$, 100 steps). TFG-4 achieves only 2.2%. Evaluation on 256 samples per species.

Species	Accuracy	FID
Lucifer Hummingbird	21.5%	24.76
Scarlet Macaw	28.1%	104.1
Fairy Tern	2.7%	93.48
Brown Headed Cowbird	3.9%	65.72
Average (Our)	14.1%	72.02
TFG-4	2.2%	259

guidance even for rare attribute combinations where the underlying model has limited training signal.

4.4 Fine-Grained Out-of-Distribution Guidance

The Fine-Grained Steering task is introduced in Ye et al. [2024] that aims to guide Imagenet models toward fine-grained concepts like certain species of birds.

Table 5 shows our Noise-Aligned RFM Steering achieves strong guidance accuracy on species with varying degrees of ImageNet representation far exceeds TFG-4 (2.2%). This demonstrates the model’s ability on controlled generation tasks. Both Scarlet Macaw and Lucifer Hummingbird achieve high accuracy (28.1% and 21.5%, respectively), demonstrating effective steering toward a species not a general superclass. For species *not* in ImageNet (Scarlet Macaw, Fairy Tern, Brown Headed Cowbird), the model generates *semantically related* bird species, demonstrating that RFM directions encode meaningful semantic structure that generalizes beyond exact class matches (sample grids in appendix, Figure 15, and some correctly generated images by our method in Figure 4).

4.5 Ablation Studies

We conduct a noise level ablation study on CIFAR-10 by training RFM classifiers at $\sigma \in \{0.6, 1.0, 1.5, 2.0, 5.0\}$ and reporting training Area Under the Curve (AUC)



Figure 4: **Fine-grained bird species guidance.** Correctly classified samples for OOD species: Lucifer Hummingbird (top-left), Scarlet Macaw (top-right), Brown Headed Cowbird (bottom-left), and Fairy Tern (bottom-right).

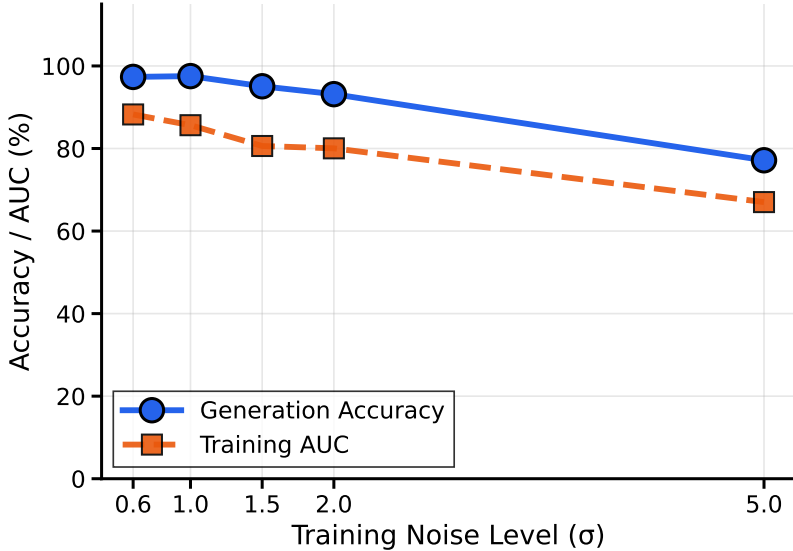


Figure 5: **Training noise level ablation.** Generation accuracy remains robust across $\sigma \in [0.6, 2.0]$, with modest degradation at $\sigma = 5.0$.

and generation accuracy. Results in Figure 5 show both metrics are stable across $\sigma \in [0.6, 1.0]$, then followed by a monotonic drop for larger $\sigma \in [1.5, 5.0]$. This supports our choice of using later low noise regime activations for direction discovery. Additional ablations and diagnostics are in the appendix: block selection (Section B), full guidance-window sweeps and timing studies (Section C), the noise-alignment accuracy–FID trade-off (Section D.2), and direction learning ablations showing RFM finds more discriminative directions than mean-difference baselines (Section D.3).

5 Discussion and Limitations

We presented NA-RFM, a framework for steering unconditional diffusion models without gradient computation at inference. Our approach leverages three observations: class information emerges early and can be exploited via noise alignment, discriminative directions from RFMs transfer effectively across timesteps, and the discriminative directions from RFMs can be used for guided generation. Experiments demonstrate substantial improvements over gradient-based methods across a range of benchmarks with high accuracy and efficiency. Some of our components, such as noise alignment, could be potentially combined to benefit other methods like gradient-based methods. It would also be interesting to see why discriminative directions as we computed are effective for generation.

6 Acknowledgement

This material is based upon work supported by the Defense Advanced Research Projects Agency (DARPA) under Contract No. HR001125CE020, and by the National Science Foundation (NSF) under grants CCF-2112665, MFAI 2502258, and MFAI 2502084; the Office of Naval Research (ONR) under grant N000142412631; We also gratefully acknowledge computational support provided through the NSF ACCESS program (allocation TG-CIS220009). We thank Xiao Lin and Yi Yao for helpful discussions.

References

- Arpit Bansal, Hong-Min Chu, Avi Schwarzschild, Soumyadip Sengupta, Micah Goldblum, Jonas Geiping, and Tom Goldstein. Universal guidance for diffusion models. In *Proceedings of the IEEE/CVF conference on computer vision and pattern recognition*, pages 843–852, 2023.
- Daniel Beaglehole, Adityanarayanan Radhakrishnan, Enric Boix-Adsera, and Mikhail Belkin. Toward universal steering and monitoring of AI models. *arXiv preprint arXiv:2502.03708*, 2025.
- Mikołaj Bińkowski, Danica J Sutherland, Michael Arbel, and Arthur Gretton. Demystifying mmd gans. *arXiv preprint arXiv:1801.01401*, 2018.
- Hyungjin Chung, Jeongsol Kim, Michael Thompson Mccann, Marc Louis Klasky, and Jong Chul Ye. Diffusion posterior sampling for general noisy inverse problems. In *The Eleventh International Conference on Learning Representations*, 2023. URL <https://openreview.net/forum?id=0nD9zGAGT0k>.
- Prafulla Dhariwal and Alexander Nichol. Diffusion models beat GANs on image synthesis. In *Advances in Neural Information Processing Systems*, volume 34, pages 8780–8794, 2021.
- Yutong He, Naoki Murata, Chieh-Hsin Lai, Yuhta Takida, Toshimitsu Uesaka, Dongjun Kim, Wei-Hsiang Liao, Yuki Mitsufuji, J Zico Kolter, Ruslan Salakhutdinov, and Stefano Ermon. Manifold preserving guided diffusion. In *The Twelfth International Conference on Learning Representations*, 2024. URL <https://openreview.net/forum?id=o3Bx0Loxm1>.
- Martin Heusel, Hubert Ramsauer, Thomas Unterthiner, Bernhard Nessler, and Sepp Hochreiter. Gans trained by a two time-scale update rule converge to a local nash equilibrium. *Advances in neural information processing systems*, 30, 2017.
- Jonathan Ho and Tim Salimans. Classifier-free diffusion guidance. *arXiv preprint arXiv:2207.12598*, 2022.
- Jonathan Ho, Ajay Jain, and Pieter Abbeel. Denoising diffusion probabilistic models. In *Advances in Neural Information Processing Systems*, volume 33, pages 6840–6851, 2020.
- Jaeseok Jeong, Mingi Kwon, and Youngjung Uh. Training-free content injection using h-space in diffusion models. In *Proceedings of the IEEE/CVF Winter Conference on Applications of Computer Vision (WACV)*, pages 5151–5161, 2024.
- Tero Karras, Timo Aila, Samuli Laine, and Jaakko Lehtinen. Progressive growing of gans for improved quality, stability, and variation. *arXiv preprint arXiv:1710.10196*, 2017.
- Tero Karras, Miika Aittala, Timo Aila, and Samuli Laine. Elucidating the design space of diffusion-based generative models. In *Advances in Neural Information Processing Systems*, volume 35, pages 26565–26577, 2022.
- Alex Krizhevsky, Geoffrey Hinton, et al. Learning multiple layers of features from tiny images. 2009.
- Mingi Kwon, Jaeseok Jeong, and Youngjung Uh. Diffusion models already have a semantic latent space. In *International Conference on Learning Representations*, 2023.
- Xiang Li, Yixiang Dai, and Qing Qu. Understanding generalizability of diffusion models requires rethinking the hidden gaussian structure. In *Advances in Neural Information Processing Systems*, 2024. URL <https://openreview.net/forum?id=Sk2duBGvrK>.

- Xiang Li, Rongrong Wang, and Qing Qu. Towards understanding the mechanisms of classifier-free guidance. *arXiv preprint arXiv:2505.19210*, 2025. URL <https://arxiv.org/abs/2505.19210>.
- Yaron Lipman, Ricky TQ Chen, Heli Ben-Hamu, Maximilian Nickel, and Matthew Le. Flow matching for generative modeling. *arXiv preprint arXiv:2210.02747*, 2024.
- Alexander Quinn Nichol and Prafulla Dhariwal. Improved denoising diffusion probabilistic models. In *International conference on machine learning*, pages 8162–8171. PMLR, 2021.
- Adityanarayanan Radhakrishnan, Daniel Beaglehole, Parthe Pandit, and Mikhail Belkin. Mechanism for feature learning in neural networks and backpropagation-free machine learning models. *Science*, 383(6690):1461–1467, 2024.
- Olga Russakovsky, Jia Deng, Hao Su, Jonathan Krause, Sanjeev Satheesh, Sean Ma, Zhiheng Huang, Andrej Karpathy, Aditya Khosla, Michael Bernstein, Alexander C. Berg, and Li Fei-Fei. ImageNet Large Scale Visual Recognition Challenge. *International Journal of Computer Vision (IJCV)*, 115(3):211–252, 2015. doi: 10.1007/s11263-015-0816-y.
- Jiaming Song, Chenlin Meng, and Stefano Ermon. Denoising diffusion implicit models. In *International Conference on Learning Representations*, 2021a.
- Jiaming Song, Qinsheng Zhang, Hongxu Yin, Morteza Mardani, Ming-Yu Liu, Jan Kautz, Yongxin Chen, and Arash Vahdat. Loss-guided diffusion models for plug-and-play controllable generation. In *International Conference on Machine Learning*, pages 32483–32498. PMLR, 2023.
- Yang Song, Jascha Sohl-Dickstein, Diederik P Kingma, Abhishek Kumar, Stefano Ermon, and Ben Poole. Score-based generative modeling through stochastic differential equations. In *International Conference on Learning Representations*, 2021b.
- Bin Xu Wang and John J. Vastola. The unreasonable effectiveness of gaussian score approximation for diffusion models and its applications. *arXiv preprint arXiv:2412.09726*, 2024. URL <https://arxiv.org/abs/2412.09726>.
- Haotian Ye, Haowei Lin, Jiaqi Han, Minkai Xu, Sheng Liu, Yitao Liang, Jianzhu Ma, James Zou, and Stefano Ermon. TFG: Unified training-free guidance for diffusion models. In *The Thirty-eighth Annual Conference on Neural Information Processing Systems*, 2024. URL <https://openreview.net/forum?id=N8YbGX98vc>.
- Jiwen Yu, Yinhuai Wang, Chen Zhao, Bernard Ghanem, and Jian Zhang. Freedom: Training-free energy-guided conditional diffusion model. In *Proceedings of the IEEE/CVF International Conference on Computer Vision*, pages 23174–23184, 2023.
- Daniel Zhao, Daniel Beaglehole, Taylor Berg-Kirkpatrick, Julian McAuley, and Zachary Noyack. Steering autoregressive music generation with recursive feature machines. *arXiv preprint arXiv:2510.19127*, 2025.

A Computational Efficiency

Beyond accuracy improvements, Noise-Aligned RFM Steering provides substantial computational speedups over gradient-based guidance. Table 6 compares wall-clock time on an NVIDIA A100-SXM4-40GB GPU for ImageNet 256×256 generation.

Table 6: **ImageNet timing comparison.** Wall-clock time for generating 4 samples with 100 DDIM steps on A100-40GB GPU. TFG configurations: TFG-1: 1 recurrence step, TFG-4: 4 recurrence steps.

Method	Time (s)
TFG-1	81.7
TFG-4	318.8
Noise-Aligned RFM Steering	31.6

Noise-Aligned RFM Steering achieves **10 ×** speedup over TFG-4. Compared to TFG-1, which achieves higher accuracy, Noise-Aligned RFM Steering is **2.5×** faster. The speedup comes from eliminating gradient computations: TFG requires backpropagation through both the diffusion model and classifier at every step, while Noise-Aligned RFM Steering uses only forward passes with a pre-computed steering direction.

B Block Selection Ablation

We compare NA-RFM guidance using features from three U-Net locations: Encoder-9 (8×8 resolution), Middle block (4×4 bottleneck), and Decoder-6 (8×8 resolution). We ablate on the *airplane* class using 256 samples to isolate the effect of block choice.

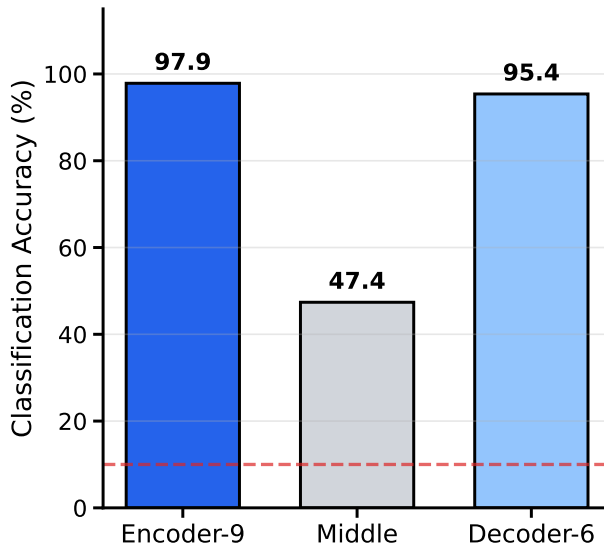


Figure 6: **Block selection ablation.** NA-RFM guidance accuracy on the *airplane* class (256 samples) for three U-Net block locations. Encoder-9 achieves highest accuracy (97.9%), with Decoder-6 comparable (95.4%), while Middle block performs poorly (47.4%). Red dashed line indicates random chance (10%).

As shown in Figure 6, both encoder and decoder blocks at 8×8 resolution achieve high accuracy (97.9% and 95.4% respectively), while the middle bottleneck block performs poorly (47.4%). This confirms that intermediate spatial resolution provides the optimal trade-off between semantic abstraction and spatial detail for guidance.

C Full Guidance Window Ablation

We investigate when guidance should be applied during the diffusion sampling process. While RFM directions are trained at a specific noise level, it is unclear whether guidance should be applied only at that noise level or across a broader range of timesteps.

Figure 7 presents a comprehensive timing window ablation with *RFM-only* guidance. We find that early-stage steering is non-consequential: steering in the second half (steps 50–99) achieves 90.2% accuracy, only 4.1% below full guidance, while steering in the first half (steps 0–49) achieves only 24.2%, barely above random. Notably, steering only near where the RFM activations are trained yields just 13.4% accuracy, essentially random, demonstrating that the guidance effect must accumulate over multiple timesteps. There is a clear monotonic relationship between the number of guided steps and final accuracy: 10 steps yields 35.2%, 20 steps yields 60.8%, 30 steps yields 75.6%, and 50 steps yields 90.2%.

D Additional Experimental Results

D.1 Timing Window Ablation

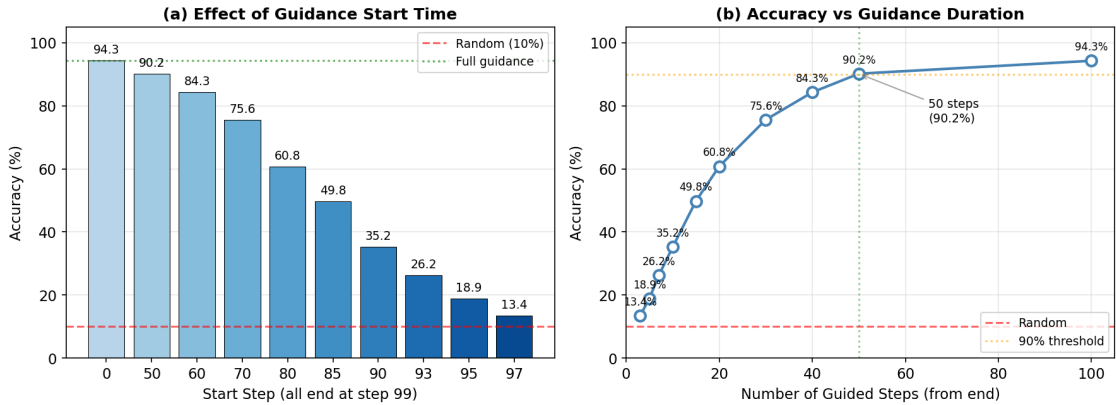


Figure 7: **Timing window ablation** (*airplane* class, 256 samples). We vary which DDIM steps receive RFM guidance. Left: Accuracy increases monotonically with the number of guided steps, with late-stage guidance (steps 50–99) being critical. Right: Early-only guidance has minimal effect, while late-only guidance captures most of the benefit. The guidance signal must accumulate over approximately 30–50 timesteps to achieve high accuracy.

D.2 Noise Alignment Ablation

Figure 8 shows the accuracy–FID trade-off for noise alignment guidance alone. Noise alignment can achieve 80% accuracy ($\lambda=10$) but with high FID (127), while $\lambda=3$ yields better quality (FID=99)

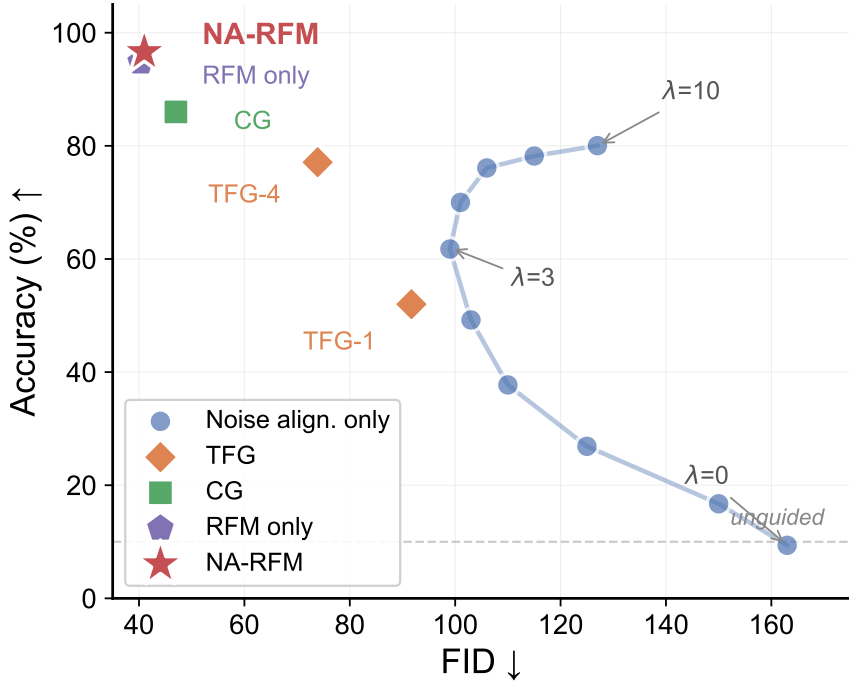


Figure 8: **Accuracy–FID trade-off for noise alignment only.** Points show noise alignment results at varying λ ; dashed line indicates Pareto frontier. Higher λ improves accuracy but degrades FID. Our full method (star) breaks through this trade-off, achieving both high accuracy and low FID.

at 62% accuracy. Our full NA-RFM breaks through this Pareto frontier, achieving 96.6% accuracy with $\text{FID}=41.4$ by combining noise alignment with RFM activation steering.

D.3 CIFAR-10 Per-Class Analysis

Per-Class Analysis. Table 7 shows per-class breakdown. NA-RFM achieves high accuracy across all 10 classes, with horse reaching 99.4%. Per-class FID ranges from 22.5 (automobile) to 62.3 (airplane).

Qualitative Visualizations. We present non-curated sample visualizations across all datasets. Figure 9 shows CIFAR-10 generations, Figures 10 and 11 show CelebA multi-attribute results, Figure 15 shows fine-grained bird species, and Figure 12 shows ImageNet generations.

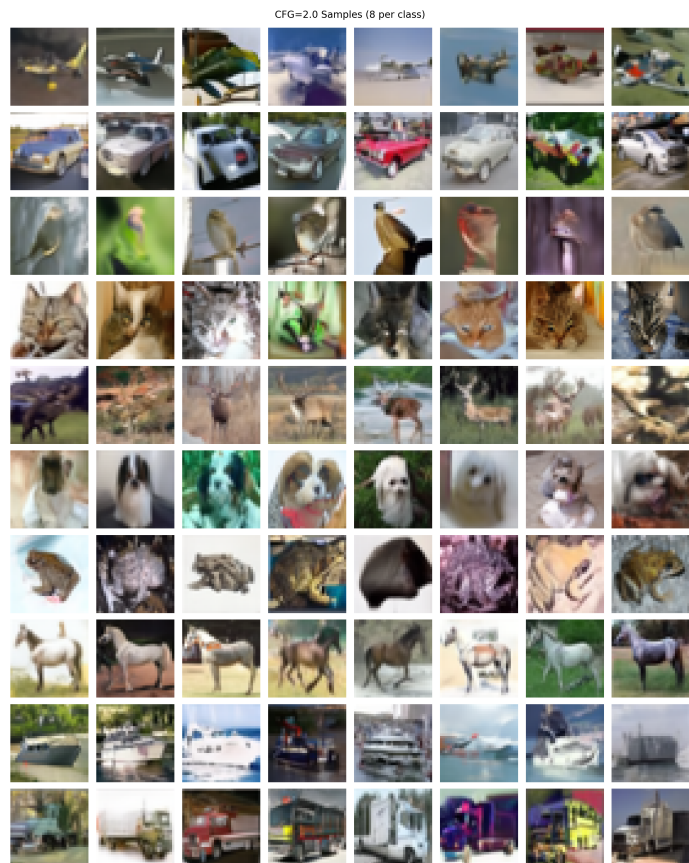


Figure 9: **CIFAR-10 samples generated with Noise-Aligned RFM Steering.** 8 samples per class, rows from top: airplane, automobile, bird, cat, deer, dog, frog, horse, ship, truck.

Table 7: **CIFAR-10 per-class results.** NA-RFM achieves consistently high accuracy across all classes with low per-class FID.

Class	Accuracy	FID
airplane	95.5%	62.3
automobile	98.1%	22.5
bird	96.2%	54.9
cat	97.2%	50.7
deer	98.4%	38.5
dog	92.1%	44.9
frog	94.6%	44.3
horse	99.4%	36.3
ship	96.9%	35.6
truck	97.4%	24.3
Average	96.6%	41.4

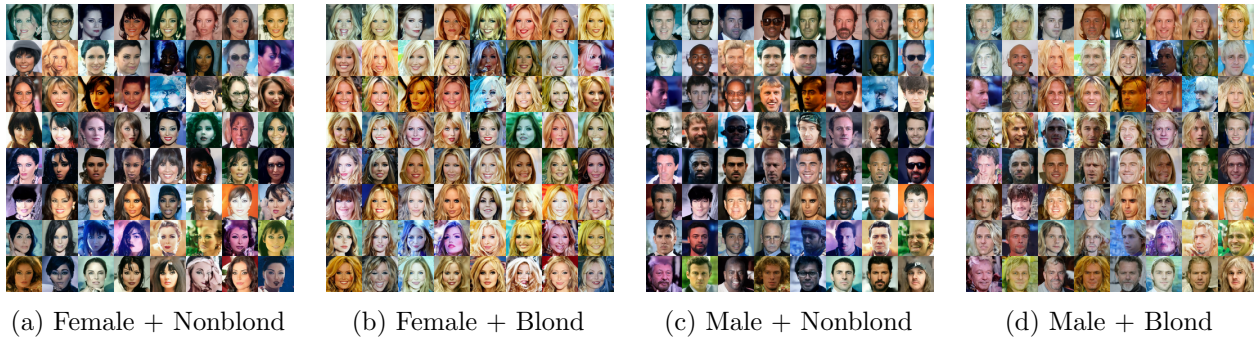


Figure 10: **CelebA Gender+Hair guidance results.** Per-combination accuracy: Female+Nonblond 86.4%, Female+Blond 80.1%, Male+Nonblond 98.4%, Male+Blond 68.4% (avg. 83.3% vs. TFG’s 75.4%).

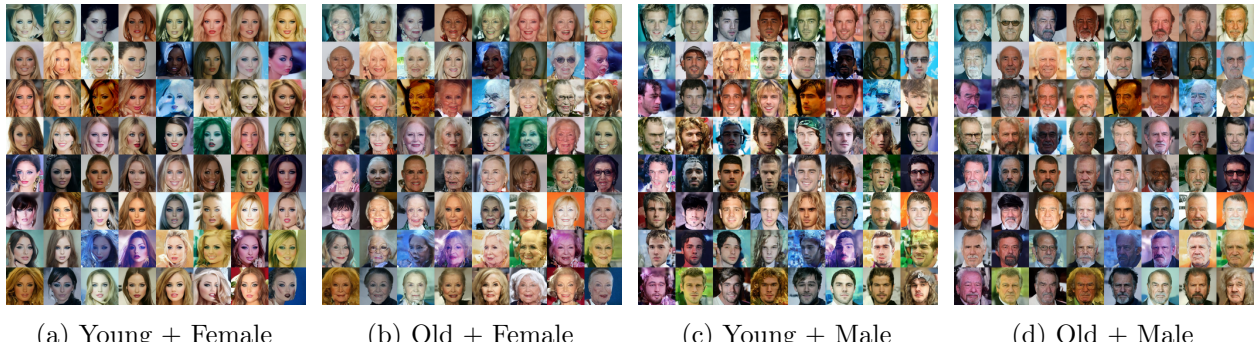


Figure 11: **CelebA Gender+Age guidance results.** Per-combination accuracy: Young+Female 100%, Old+Female 85.2%, Young+Male 98.8%, Old+Male 100% (avg. 96.0% vs. TFG’s 82.3%).

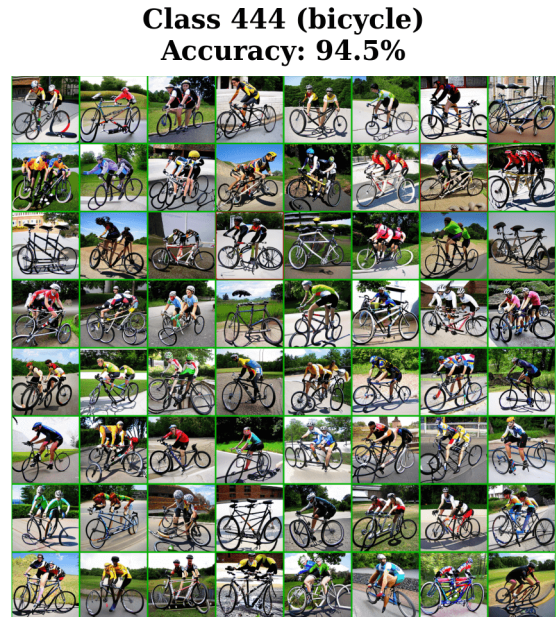
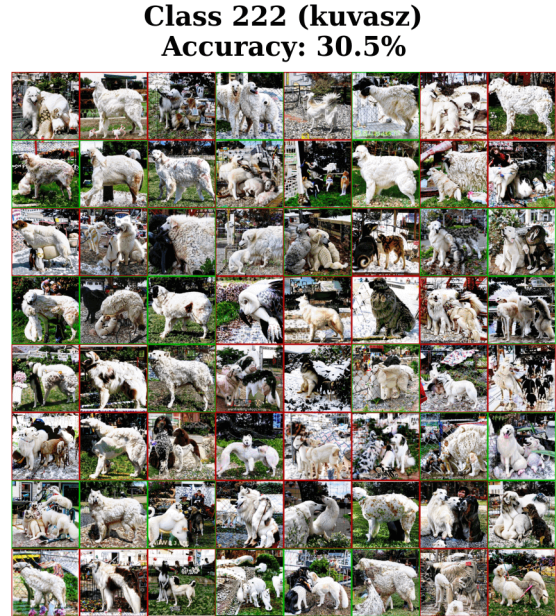
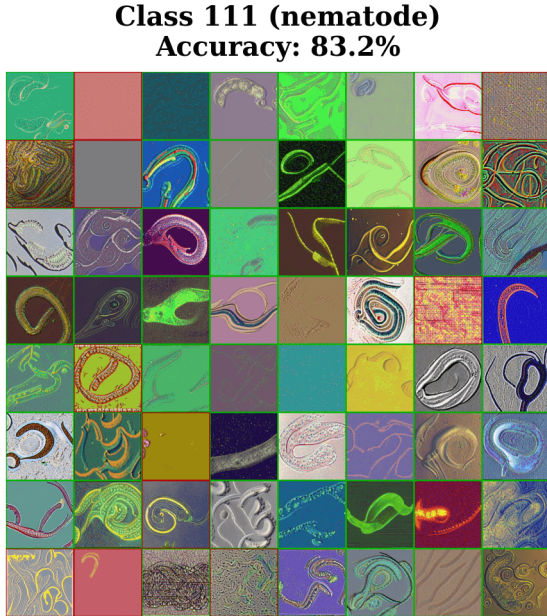


Figure 12: **ImageNet label guidance sample grid.** Generated samples for four target classes (Nematode, Kuvasz, Hamster, Tandem Bicycle) using our best guidance methods. Each class shows an 8×8 grid of samples, demonstrating successful semantic steering and sample diversity across target concepts.

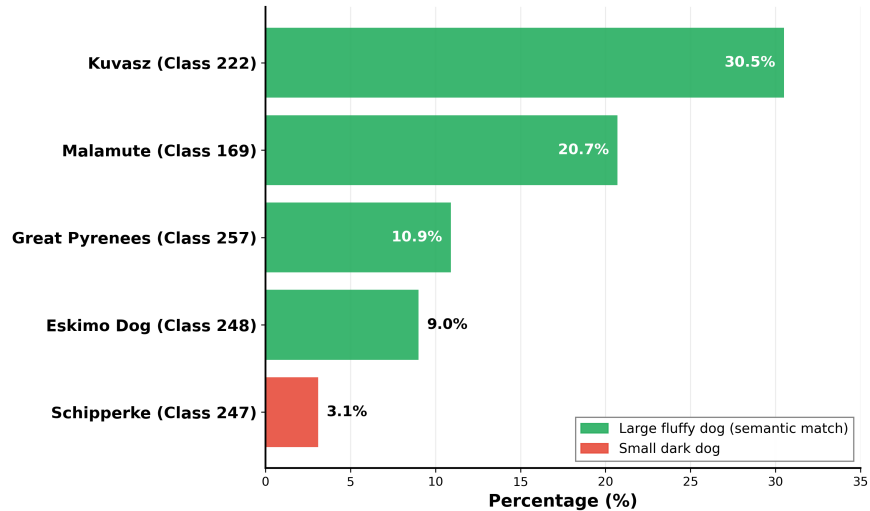


Figure 13: **Class 222 (Kuvasz) confusion analysis.** Top predictions show successful semantic steering: the top 4 classes (71.1% of samples) are all large, light-colored, fluffy dogs—Kuvasz (30.5%), Malamute (20.7%), Great Pyrenees (10.9%), and Eskimo dog (9.0%). Top-5 accuracy of 74.2% demonstrates that our method correctly steers to the target semantic category, with confusion only among visually similar breeds.

Direction Learning Ablation: Mean Difference vs. RFM. We compare our learned RFM directions against a simpler baseline: mean difference directions computed as $\mathbf{d} = \mathbb{E}[\mathbf{h}|y = c] - \mathbb{E}[\mathbf{h}]$, where \mathbf{h} denotes intermediate activations. This baseline represents a “centroid” approach that captures the average direction toward a class (Table 8 and Figure 14).

Table 8: **Direction learning ablation on ImageNet Kuvasz (class 222).** RFM directions achieve 5× higher accuracy and produce diverse poses, while mean difference directions collapse to a fixed pose template.

Method	Acc.	Confidence	Pose Diversity
Mean Diff. steering	6.2%	0.08	Low (fixed template)
RFM steering (Ours)	30.5%	0.24	High (varied poses)

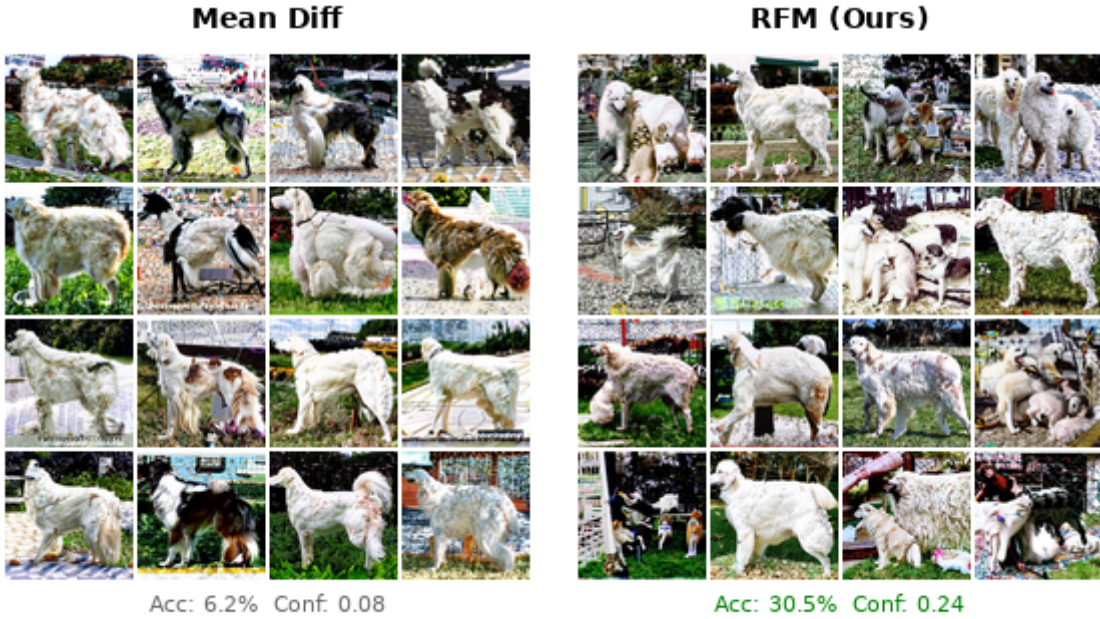
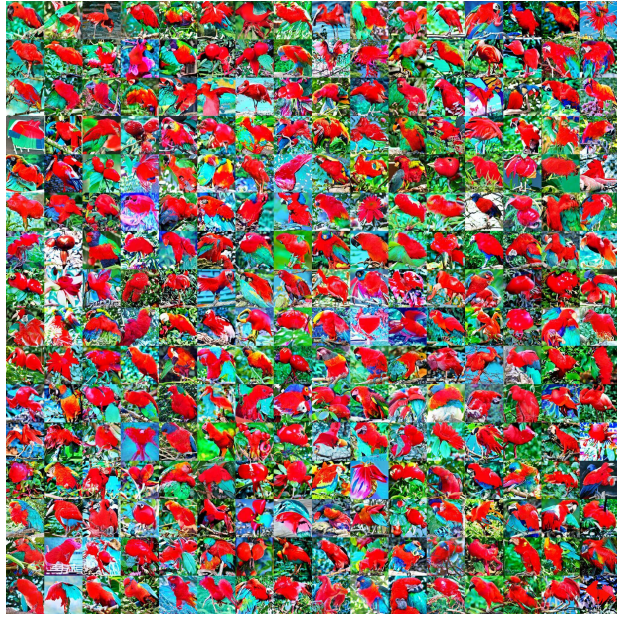


Figure 14: **Mean difference vs. RFM direction comparison on Kuvasz (class 222).** *Left:* Mean difference guidance produces dogs with nearly identical standing profile poses—the direction captures only a single “average” pose. *Right:* RFM guidance produces diverse poses (sitting, standing, lying, multiple angles) while achieving 5× higher classification accuracy.

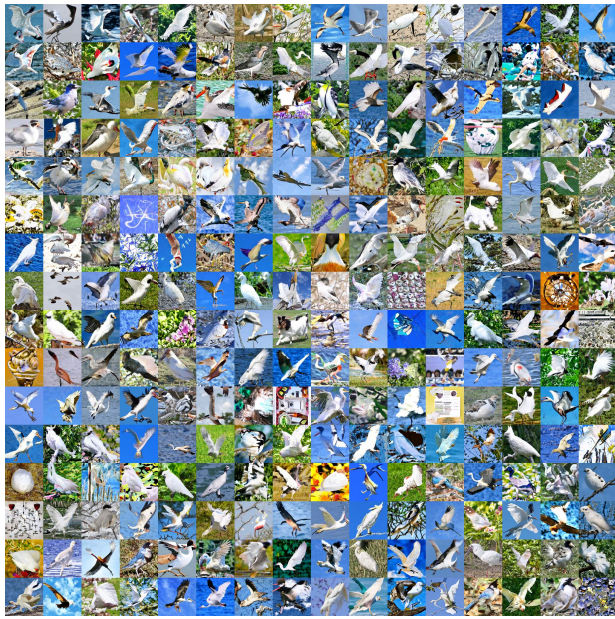
The mean difference approach may fail for two reasons: (1) it averages over all class instances, collapsing pose and viewpoint diversity into a single template, and (2) this fixed direction does not generalize well during generation, achieving only 6.2% accuracy. In contrast, RFM learns a semantic direction that better captures the natural diversity of the target class while achieving substantially higher guidance accuracy.



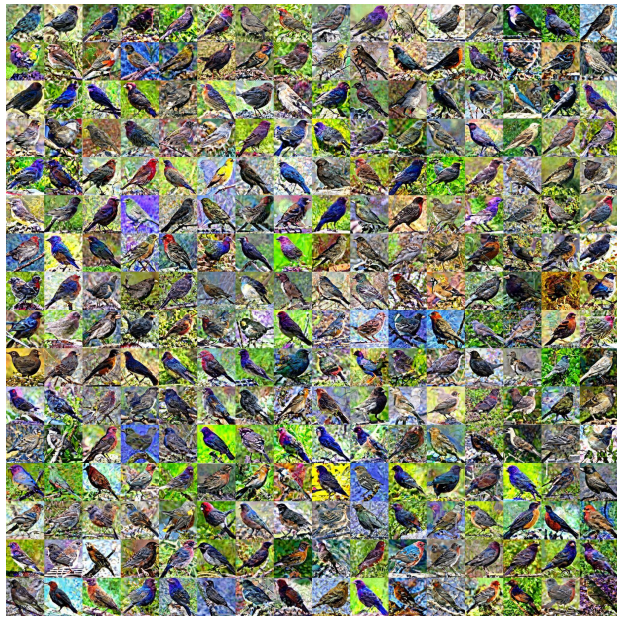
(a) Lucifer Hummingbird (21.5%)



(b) Scarlet Macaw (28.1%)



(c) Fairy Tern (2.7%)



(d) Brown Headed Cowbird (3.9%)

Figure 15: **Fine-grained bird species generation samples.** Non-curated samples generated using deterministic DDIM sampling (100 steps). Percentages indicate target species accuracy on 256 samples using Birds-525 classifier.

E Implementation Details

We provide detailed implementation specifications for reproducibility. All experiments use deterministic DDIM sampling with $\eta = 0$ and 100 inference steps unless otherwise noted.

Model Checkpoints and Architecture. Table 9 lists the diffusion model checkpoints used across

all experiments.

Table 9: **Diffusion model checkpoints and architectures.**

Dataset	Architecture	Checkpoint URL
CIFAR-10	Improved DDPM U-Net	https://openaipublic.blob.core.windows.net/diffusion/march-2021-ema/cifar10_uncond_50M_500K.pt
ImageNet	ADM U-Net (256×256)	https://openaipublic.blob.core.windows.net/diffusion/jul-2021/256x256_diffusion_uncond.pt
CelebA-HQ	DDPM U-Net	https://huggingface.co/google/ddpm-celebahq-256

The ImageNet ADM architecture uses: 256 base channels, channel multipliers [1, 1, 2, 2, 4, 4], 2 residual blocks per resolution, attention at 32×32, 16×16, and 8×8 resolutions, 64 channels per attention head, and learned sigma prediction.

Guidance and Evaluation Classifiers. We use separate classifiers for guidance (labeling training data) and evaluation (measuring generation accuracy) to prevent inflated results. See Tables 10 and 11.

Table 10: **Guidance classifiers** used for labeling data when the label is not available.

Dataset	Architecture	Source
CIFAR-10	ResNet-18	OpenOOD benchmark
ImageNet	ViT-B/16	torchvision pretrained
CelebA (Age)	ViT	https://huggingface.co/nateraw/vit-age-classifier
CelebA (Gender)	ViT	https://huggingface.co/rizvandwiki/gender-classification-2
CelebA (Hair)	ViT	https://huggingface.co/enzostvs/hair-color
Birds-525	EfficientNet	https://huggingface.co/chriamue/bird-species-classifier

Training Data for Direction Discovery. Table 12 summarizes the datasets used for computing PCA statistics and RFM directions.

Per-Dataset Implementation Details. We provide full hyperparameters for each dataset below. Table 13 covers CIFAR-10, Table 14 covers ImageNet, Tables 15 and 16 cover CelebA-HQ, and Tables 17 and 18 cover fine-grained bird species.

Timestep and Noise Level Correspondence. For CIFAR-10 (linear β schedule with 100-step DDIM), we collect at DDIM step 93, which maps to DDPM timestep $t = 60$:

$$\bar{\alpha}_{60} = \prod_{i=1}^{60} (1 - \beta_i) \approx 0.958, \quad \sigma_{60} = \sqrt{\frac{1 - \bar{\alpha}_{60}}{\bar{\alpha}_{60}}} \approx 0.21 \quad (12)$$

Table 11: **Evaluation classifiers** (used for evaluating guidance accuracy).

Dataset	Architecture	Source
CIFAR-10	ConvNeXT-Tiny	https://huggingface.co/ahsanjavid/convnext-tiny-finetuned-cifar10
ImageNet	DeiT-Small	https://huggingface.co/facebook/deit-small-patch16-224
CelebA (Age)	Swin	https://huggingface.co/ibombonato/swin-age-classifier
CelebA (Gender)	ViT	https://huggingface.co/rizvandwiki/gender-classification
CelebA (Hair)	ViT	https://huggingface.co/londe33/hair_v02
Birds-525	EfficientNet-B2	https://huggingface.co/dennisjooo/Birds-Classifier-EfficientNetB2

Table 12: **Training data** used for computing PCA statistics and RFM directions.

Dataset	Size	Source
CIFAR-10	50,000 images	<code>torchvision.datasets.CIFAR10</code>
ImageNet-1k	1.28M images	https://huggingface.co/datasets/imagenet-1k
CelebA-HQ	30,000 images	https://github.com/tkarras/progressive_growing_of_gans
Birds-525	89,885 images	https://huggingface.co/datasets/chriamue/bird-species-dataset

Table 13: **CIFAR-10 implementation details.**

Parameter	Value
<i>Diffusion Model</i>	
Architecture	OpenAI U-Net (improved DDPM)
Image resolution	32×32
Noise schedule	Linear $\beta \in [0.0001, 0.02]$, 1000 steps
<i>Activation Collection</i>	
U-Net block	<code>input_blocks_9</code>
Feature map resolution	8×8
Collection timestep	DDIM step 93 out of 100 steps
Samples per class	1,000
Training data	CIFAR-10 train split (50,000 images)
<i>RFM Training</i>	
Kernel	ℓ_2 (Laplacian)
Bandwidth	100
Regularization	10^{-3}
Iterations	5
Top- k eigenvectors	3
<i>Guidance Settings</i>	
RFM window	Steps 30–99
RFM strength w_{RFM}	0.235
Noise alignment window	Steps 0–50
Noise alignment λ	7.0

 Table 14: **ImageNet implementation details.**

Parameter	Value
<i>Diffusion Model</i>	
Architecture	ADM U-Net (unconditional)
Image resolution	256×256
Noise schedule	Cosine schedule, 1000 steps
<i>Activation Collection</i>	
U-Net block	<code>input_blocks_15</code>
Feature map resolution	8×8
Feature channels	1024
Collection noise level	$\sigma \approx 1.0$
Training data	ImageNet-1k train split (in training we use 1,300 target classes + 15,000 random classes)
<i>RFM Training</i>	
Kernel	ℓ_2 (Laplacian)
Bandwidth	200
Regularization	10^{-4}
Iterations	5
Top- k eigenvectors	1
<i>Guidance Settings (per-class optimized)</i>	
Class 111 (nematode)	$s=12, \lambda=2, \sigma_{\text{end}}=3, w_{\text{RFM}}=0.5, \sigma_{\text{R}}^{\text{hi}}=30$
Class 222 (Kuvasz)	$s=8, \lambda=2, \sigma_{\text{end}}=2, w_{\text{RFM}}=1.0, \sigma_{\text{R}}^{\text{hi}}=80$
Class 333 (hamster)	$s=4, \lambda=1, \sigma_{\text{end}}=10, w_{\text{RFM}}=0.5, \sigma_{\text{R}}^{\text{hi}}=80$
Class 444 (bicycle)	$s=12, \lambda=2, \sigma_{\text{end}}=7, w_{\text{RFM}}=0.7, \sigma_{\text{R}}^{\text{hi}}=80$

Table 15: **CelebA-HQ** implementation details.

Parameter	Value
<i>Diffusion Model</i>	
Architecture	DDPM U-Net
Image resolution	256×256
Model checkpoint	google/ddpm-celebahq-256
<i>Activation Collection</i>	
U-Net block	<code>input_blocks_15</code>
Feature map resolution	8×8
Collection noise level	$\sigma \approx 1.0$
Training data	CelebA-HQ 256×256 (30,000 images)
<i>Attribute-Specific Training Data</i>	
Gender	Female: 18k, Male: 10k
Age	Young: 20k, Old: 1.9k
Hair color	Black: 8k, Blond: 9k
<i>RFM Training</i>	
Kernel	ℓ_2 (Laplacian)
Bandwidth	150
Regularization	10^{-3}
Iterations	5
Top- k eigenvectors	5
<i>Guidance Settings (shared)</i>	
Noise alignment λ	2.0
Noise alignment window	$\sigma \geq 3.5$
CFG scale s	2.0
RFM strength w_{RFM}	0.4
RFM window	$0.5 \leq \sigma < 3.5$

 Table 16: **Per-attribute guidance settings for CelebA multi-attribute guidance.** Each attribute has independent λ and w_{RFM} scaled from base values by $\alpha \in \{0.25, 0.5, 1.0\}$.

Combination	λ_1	$w_{\text{RFM}}^{(1)}$	λ_2	$w_{\text{RFM}}^{(2)}$	Accuracy
<i>Gender + Hair Color</i>					
Male + Blond	1.0	0.2	2.0	0.4	68.4%
Male + Non-Blond	1.0	0.2	0.5	0.1	98.4%
Female + Blond	1.0	0.2	1.0	0.2	80.1%
Female + Non-Blond	0.5	0.1	0.5	0.1	86.4%
<i>Gender + Age</i>					
Young + Female	1.0	0.2	1.0	0.2	100.0%
Old + Female	2.0	0.4	1.0	0.2	85.2%
Young + Male	1.0	0.2	1.0	0.2	98.8%
Old + Male	2.0	0.4	2.0	0.4	100.0%

Table 17: **Birds-525** fine-grained implementation details.

Parameter	Value
<i>Diffusion Model</i>	
Architecture	ADM U-Net (same as ImageNet)
Image resolution	256×256
<i>Activation Collection</i>	
U-Net block	<code>input_blocks_15</code>
Feature map resolution	8×8
Collection noise level	$\sigma \approx 1.0$
Training data	Birds-525 (HuggingFace) 160 images per class
<i>RFM Training</i>	
Kernel	ℓ_2 (Laplacian)
Bandwidth h	200
Regularization λ_{reg}	10^{-4}
Iterations	5
Top- k eigenvectors	5
<code>center_grads</code>	true
<i>Target Species</i>	
Lucifer Hummingbird	Partial ImageNet overlap (“hummingbird” class)
Scarlet Macaw	Not ImageNet Class
Fairy Tern	Not ImageNet Class
Brown Headed Cowbird	Not ImageNet Class
<i>Sampling</i>	
Sampler	DDIM
Steps	100
η	0.0
RFM window	Steps 10–90
Samples per evaluation	256

Table 18: Per-species guidance settings for Birds-525.

Species	s	w_{RFM}	λ	σ_{end}	Accuracy
Lucifer Hummingbird	5.0	0.7	3.0	10.0	21.5%
Scarlet Macaw	5.0	0.3	3.0	10.0	28.1%
Fairy Tern	3.0	0.3	2.0	10.0	2.7%
Brown Headed Cowbird	5.0	0.5	1.0	2.0	3.9%